

Research Article

Assessment of Fractures in Excavation Damaged Zone around Roadways of an Iron Mine Using Optical Televiewer Detecting Method

Fengyu Ren , Xialiang Qiao , and Jianli Cao 

School of Resources and Civil Engineering, Northeastern University, Shenyang 110000, Liaoning Province, China

Correspondence should be addressed to Xialiang Qiao; 1610338@stu.neu.edu.cn

Received 20 November 2021; Revised 11 January 2022; Accepted 25 February 2022; Published 13 October 2022

Academic Editor: Guang-Liang Feng

Copyright © 2022 Fengyu Ren et al. This is an open access article distributed under the Creative Commons Attribution License, which permits unrestricted use, distribution, and reproduction in any medium, provided the original work is properly cited.

The properties of the excavation damaged zone (EDZ) are critical to the stability of the surrounding rock masses of the chamber, roadway, and dam, and fractures in the EDZ also affect the properties of the EDZ. In this paper, the fractures in the EDZ of an underground iron mine roadway were tested using borehole television (BTV). The results revealed that the better the grade of rock mass is, the less broken it was after excavation. An assessment method based on BTV image data has been proposed for evaluating the roadway's surrounding rock. This method uses the borehole image data to classify the excavated surrounding rock into intact rock mass, joint zone, fracture zone, and broken zone based on the condition of rock and the distribution of fractures within the rock mass. A relatively complete joint zone caused by the construction of the drill and blast method was found by using this method, and the support measures should ensure that this joint zone is not damaged. The method provides a better basis for improving the support design, according to which the improved support measures have achieved a better support effect and economic benefits.

1. Introduction

With the increasing demand for infrastructure construction as the global economy progresses, various projects are planned, are under construction, or have been built [1–3]. The excavation damaged zone (EDZ) is widely concerned with the construction of infrastructure, such as construction of large underground caverns, the stability of dam foundations, and the disposal of nuclear waste. The safety of roadways is one of the most critical issues in mining engineering. The existence of EDZ and fractures in it has a vital influence on maintaining the stability of roadways and reducing the cost of support.

Studies on the definition, mechanical and hydraulic properties, and extent of EDZ have been extensively discussed by many researchers in the past decades. There are many different definitions of EDZ under different testing methods and rock types. Two main conceptions of the EDZ definition are: (i) The EDZ is a zone in which hydromechanical and

geochemical modifications induce significant changes in flow and transport properties [4]. (ii) The excavation damaged zone (EDZ) is a zone with significant irreversible processes and significant changes in flow and transport properties [5].

On the basis of previous studies, scientists have continuously studied EDZ by adding short- and long-term strength, dilatancy, damage, and healing into constitutive model, introducing a series of methods such as separated tensile and compressive damage functions, rock permeability change functions, shear strain localization bands, maximum tensile strain criterion and so on. The shape, extent, and spatial-time characteristics of EDZ predicted by them provide some reference value for solving the field problems [6–10].

Although mechanical analysis reflects the development, behavior, shape, and extent of EDZ, field testing is still the most effective and reliable method to study EDZ. Switzerland, Sweden, South Korea, France, Japan, China, and other countries have carried out a lot of field tests of EDZ in recent

years. With methods of laboratory tests, borehole radar reflection survey, and empirical equation calculation, S. Kwon et al. [11] estimated the EDZ of the Korea Atomic Energy Research Institute underground research tunnel (KURT). L. Malmgren et al. [12] investigated the EDZ of Kiirunavaara mine by seismic measurements. As a complement, borehole image processing systems show the fractures in EDZ commendably as well. Other scientists detected the EDZ of the Mont Terri tunnel in France with the complex resistivity method and mini-sonic borehole probe. This EDZ is about 1 m thick on the roof. Its thickness decreases to about 0.5 m on the sidewall [13, 14]. The methods above are the most popular methods for EDZ measurement in the world. P. Bossart et al. [15] got the characteristics of fractures by analyzing resin-injected overcores taken from the EDZ. They introduced a conceptual model of EDZ that consists of an outer plastic zone with isolated fractures and an inner plastic zone with an air-filled fracture network. This result is in line with the research by Wu et al. [16] that analyses the strain energy of unloading to quantify the extent and degree of damage of EDZ. They put forward the conclusion that EDZ can be divided into excavation heavily disturbed subzone (EHDZ) and excavation slightly disturbed subzone (ESDZ) according to the variation of unloading strain. Bluemling P. et al. [17] considered that stress redistribution will lead to the creation of EDZ and the extent of it is decided by the initial stress field, the material properties, the existence of natural fracture zones, and the geometry of the tunnel. They think that the development of EDZ can be controlled with appropriate and timely support, although short-term failure cannot be avoided. T. Sato et al. [18] measured the vibration and seismic refraction of Tono Mine in Japan. They came up with the conclusion that the extent of EDZ is also related to excavation methods such as mechanical excavation and blasting. The conclusion that an EDZ is unnecessary in a mechanical excavation model is similar to the point of view that mechanical damage does not always result in a significant change in hydraulic properties due to self-sealing processes occurring in claystone held by G. Armand et al. [19].

It is not always easy to have a field test of EDZ due to the limitation of site conditions. The development of computers in recent decades has made it possible to simulate EDZ. Microseismic and acoustic emission events are considered to be indicators of rock mass damage, and FLAC and PFC software allow us to simulate this situation. Some scientists have simulated the stress-strain distribution of rock masses using the FLAC/PFC coupled approach [20, 21]. Some scientists also use the realistic failure process analysis (RFPA) code to discuss the failure process in the EDZ of rock mass [22]. Some scholars who focus on the effects of blasting use LS-DYNA software to simulate the damage behavior of rocks under the common effect of stress redistribution and blasting [23]. In addition, the finite element code CAST3M developed by the French Atomic Energy Commission (CEA) is also used to simulate the extent and influence of EDZ [24].

In this study, field tests were carried out to evaluate fractures in EDZ in Xingshan iron mine. An assessment

method of roadway surrounding rock based on BTV image data is proposed, which classifies the excavated rock mass according to the condition of rock and the distribution of fractures within the rock mass. A joint zone within 1.5 m of the roadway was found by using this assessment method. The improved support measures were proposed based on analysis of the possible causes of the joint zone.

2. Background

2.1. Engineering Background. The assessment of fractures in EDZ was conducted in the Xingshan underground iron mine, Hebei Province, China (Figure 1). The Xingshan iron mine is an underground mine with an annual production of 3.2 million tons of iron ore. Damaged by the F9 fault, the orebody is divided into two parts: Daxingshan and Xiaoxingshan. Daxingshan strikes 40° northeast and dips 60° to the southeast. It is 440 m long and 120 m wide on average and extends from the depth of -30 m to -610 m. Xiaoxingshan strikes at 65° southeast and dips at 45° to the southwest. It is 450 m long and 40 m wide on average. The height of the sublevel is 18.75 m, the drift is perpendicular to the strike of the orebody, and the drift interval is 20 m (Figure 2). $3^\#$ mining area is a part of Daxingshan.

The engineering geological characteristics of the deposit are general. The quality of the surrounding rock of Xingshan iron mine is generally good through the point load test and structural plane investigation (Figure 3). The basic quality of a specific rock is shown in Table 1. The hydrogeological conditions of the mining area are simple, and there is no large-scale aquifer.

2.2. Geology of the Ore Deposit. The orebody of the Xingshan iron mine lies in a sedimento-metamorphic lean iron-bedded deposit. The hanging consists wall mainly of garnet-biotite gneiss and pyroxene-biotite gneiss, while the footwall consists of biotite-plagioclase gneiss and sillimanite-garnet quartzite. The occurrence of hanging wall and footwall is consistent with that of the orebody, and the ore-rock boundary is obvious. The intercalated rocks are mainly iron-containing gneiss and iron-containing pyroxene quartzite. The main iron ore consists of magnetite and pyrite, with a Fe content of 33.2%.

2.3. Excavation Method. The roadways (crosscut or haulage drift) of Xingshan iron mine are excavated by the drill and blast method. It is in the shape of three center arches, with a size of 4.8 m * 3.9 m. The number of blast holes is determined to be 51 (including 47 charging holes and 4 non-charging holes) according to the Protogyakonov's coefficient of rock strength ($f=12$) and the roadway section area ($S=17.43\text{ m}^2$). The minimum burden is determined by the diameter of the blast hole. The holes were laid out according to the principle that the auxiliary holes (6–24) were evenly laid out in the section and the periphery holes (25–51) were laid out in the contour line. The footage of each blast is 2.8 m (Figure 4).

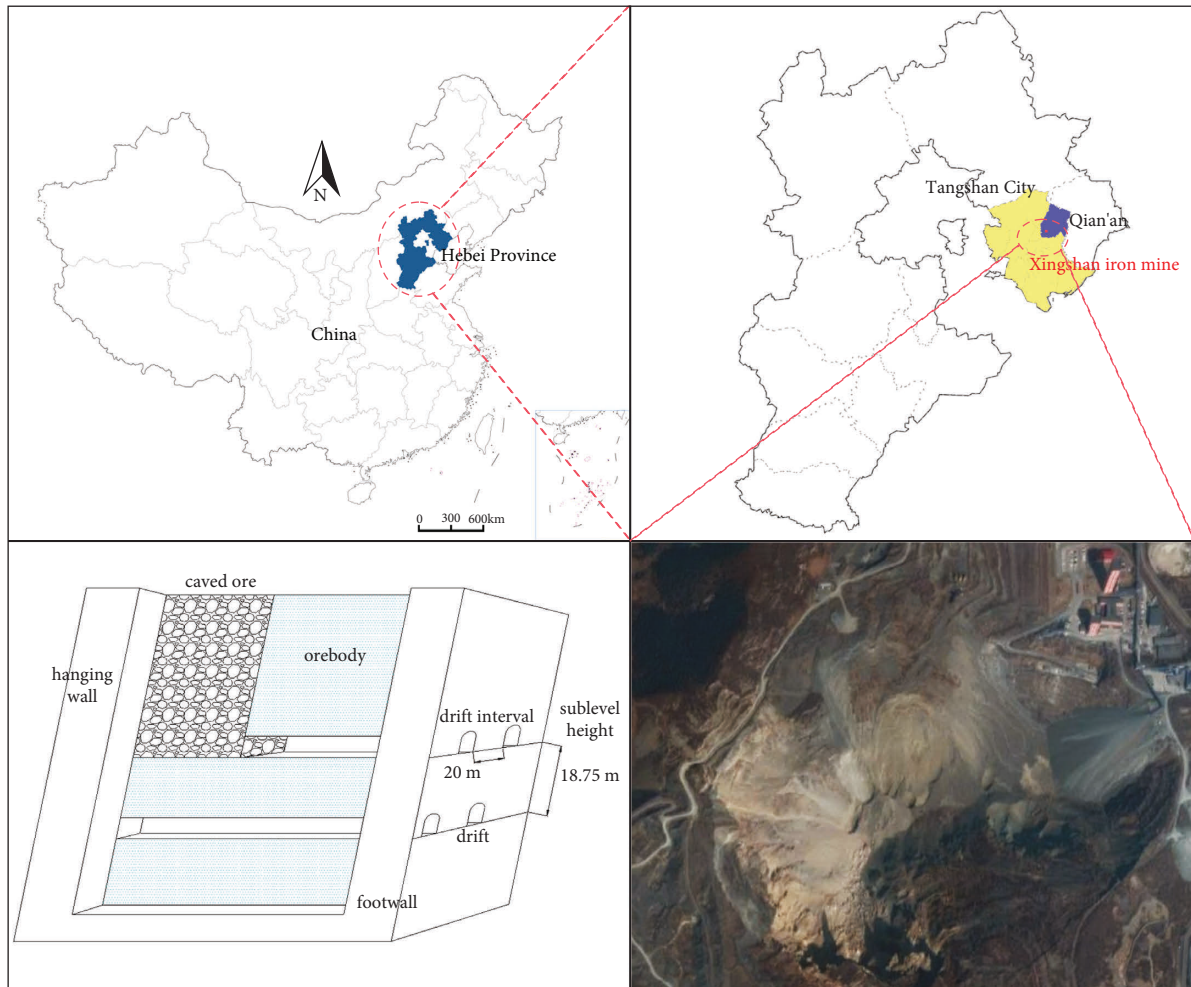


FIGURE 1: Location map of Xingshan iron mine.

2.4. Support System. In Xingshan iron mine, a shotcrete-bolt-net supporting system is adopted to support the surrounding rock. The support sequence is as follows: initial shotcrete is carried out first, then metal net is hung, bolt support is installed, and finally secondary shotcrete is carried out. The length of the bolt is 2.0 m, the spacing of the bolt is 1.2 m, and the row spacing is 1.2 m. The metal mesh is welded with $\Phi=6$ mm steel bar. The grid is 150 mm * 150 mm size with a diamond shape.

2.5. Applications of BTV Methods for EDZ Investigation.

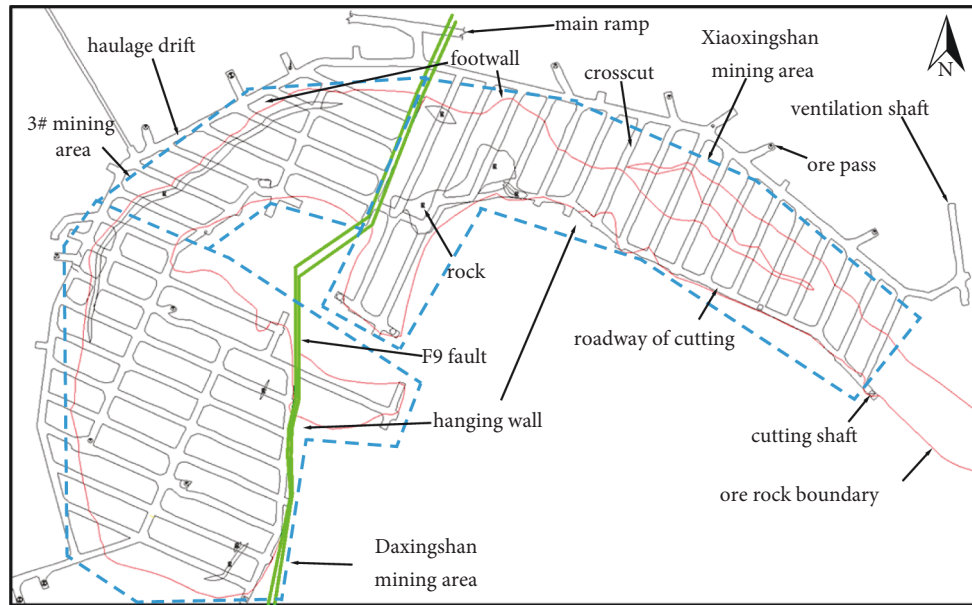
At first, scientists mainly used multipoint extensometers to measure the extent of EDZ. With an increasing understanding of EDZ, acoustic wave and cross-hole seismic techniques were used to investigate the EDZ of collieries prevalently. The application of the borehole television method in the survey of EDZ was used around 2000, and it emerged in the last ten years. Japanese scientists developed the borehole image processing system that made it possible to survey tunnel fractures by BTV in 1990 [25]. In the last decade, Feng and his team used BTV to measure the EDZ of tunnels in Jinping, Baihetan, and other places. They studied the evolutionary process of fractures in EDZ and the EDZ change process over time, proposed a new rock mass

integrity evaluation method based on high-definition digital borehole televiewer data, and solved the problems in the design of tunnel excavation and supports [26–32]. In recent years, scientists have also used BTV to analyze the influence of TBM excavation, complex geological conditions, dynamic pressure induced by active mining processes, and other aspects of EDZ [33–36]. In general, the use of BTV enables us to obtain and record information such as the condition, width, and orientation of fractures in the roadway surrounding rock intuitively, which is of great help to analyze the formation of EDZ and reducing its influence.

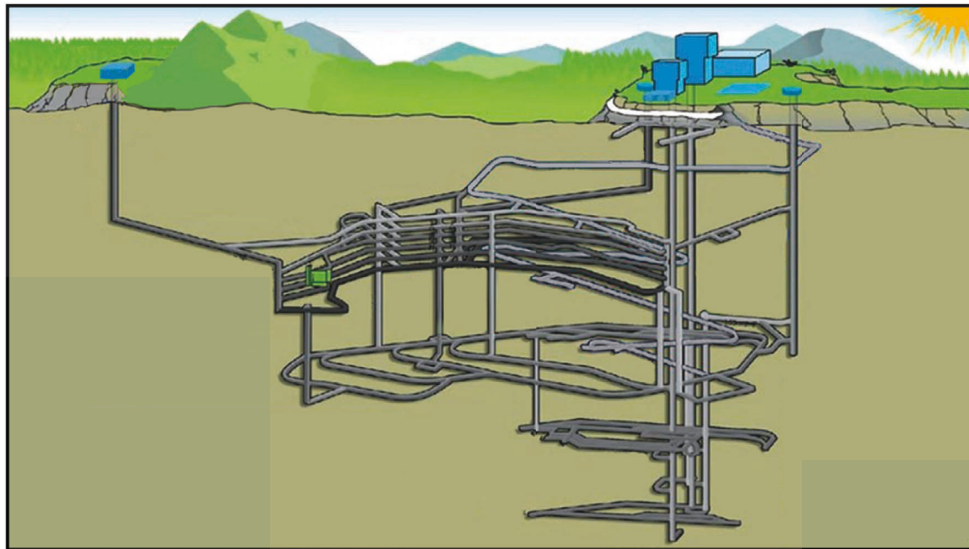
3. Measurement

3.1. Test Area. Fractures in EDZ field tests were carried out at -218 m sublevel and -236 m sublevel in Xingshan iron mine (Figure 5). The test location includes the hanging wall, orebody, and footwall of the Daxingshan mining area, 3[#] mining area, and Xiaoxingshan mining area (Table 2).

3.2. Test Equipment. The equipment consists of four main parts, which are the surface acquisition system, software, winch and cable, and probe. The probe is an optical televiewer sonde, which is a white-light borehole imaging sonde.



(a)



(b)

FIGURE 2: Layout of Xingshan iron mine (a) plan of typical sublevel layout (b) schematic diagram of shaft and roadway positions of Xingshan iron mine.

The image of the borehole wall is recorded as a 360° continuous projection in the log file as a series of 24 bit RGB values and transmitted to the surface system. The post-processing software RGLDIP 6.2 (Robertson Geologging, Ltd., UK) is used to process the dip and strike of borehole wall features, the status of cracks and joint planes, along with other geological conditions.

3.3. Methods. Combined with the existing works of Xingshan iron mine, vertical boreholes of $\Phi 90$ mm were constructed upward on the roof of the roadway, and horizontal boreholes were constructed on the sidewall, and the location of the borehole must ensure that both ends of the borehole

connect two roadways. Therefore, the vertical borehole must penetrate the middle of the upper sublevel roadway floor, and the horizontal borehole must penetrate the adjacent roadway (Figure 6). A total of 23 measurement points were arranged, including 17 vertical boreholes, numbered 1–17, and 6 horizontal boreholes, numbered 18–23 (Figure 5). The equipment and its arrangement are shown in Figure 7.

For a vertical borehole, the RG probe is probed from the top down. First of all, a capstan is placed on the hole position. The capstan should be ensured to be above the hole so that the probe can be lowered by gravity. Then the winch and the probe are connected so that the probe can be lowered along the axis of the test hole. Finally, open the PC and slowly lower the probe to measure the hole wall image.

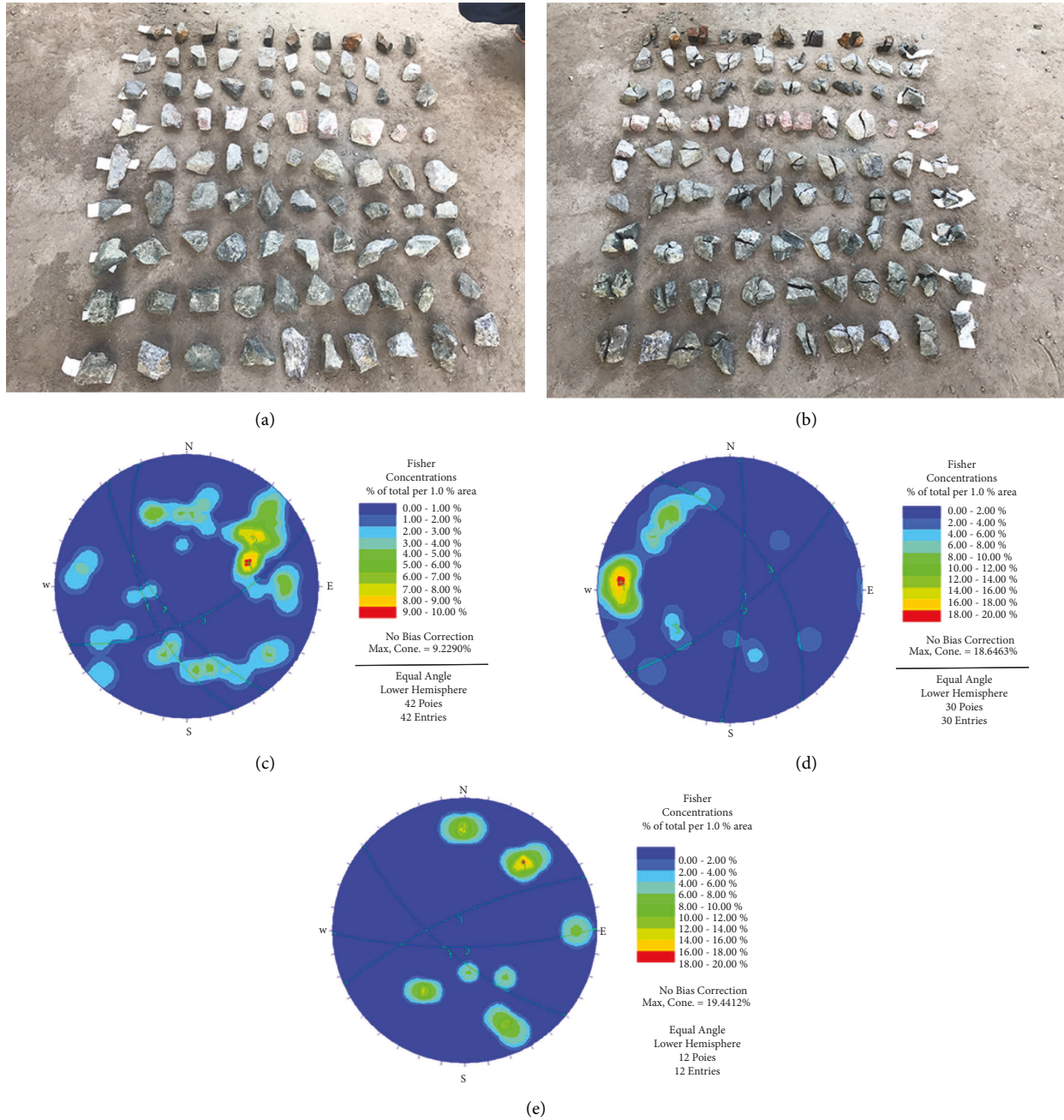


FIGURE 3: Rock mass quality classification test. (a) Point load test sample, (b) sample after test, (c) pole contour map of Xiaoxingshan footwall, (d) pole contour map of Daxingshan orebody, and (e) pole contour map of 3[#] mining area hanging wall.

TABLE 1: Ore-rock stability classification of Xingshan iron mine.

Location		Basic quality of rock mass Q	Classification of stability
Xiaoxingshan mining area	Hanging wall	321–450	IV–III
	Orebody	277–633	IV–I
	Footwall	238–560	V–I
3 [#] mining area	Hanging wall	353–664	III–I
	Orebody	386–444	III
	Footwall	285–521	IV–II
Daxingshan mining area	Hanging wall	290–595	IV–I
	Orebody	277–575	IV–I
	Footwall	273–398	IV–III

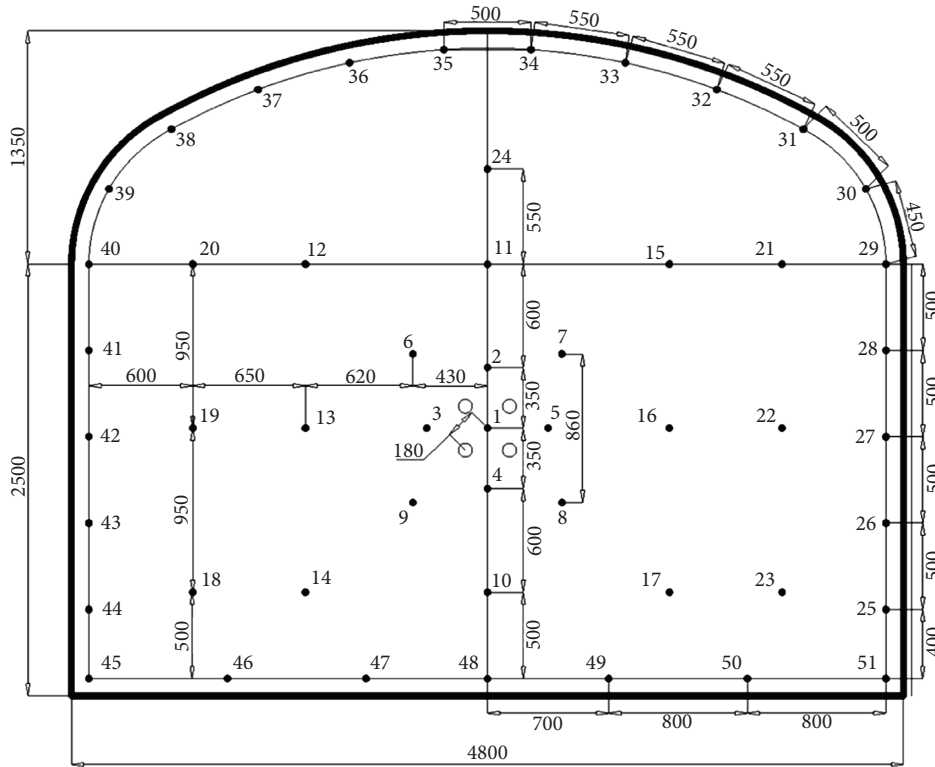


FIGURE 4: Blast hole layout of the Xingshan iron mine roadway (mm).



FIGURE 5: EDZ test position on the roof or sidewall. (a) -218 m sublevel. (b) -236 m sublevel.

For the horizontal borehole on the sidewall, the tripod should be set up on the roadway side, the length of the tripod legs should be adjusted appropriately, and the winch, power source, and other equipment should be placed in the appropriate position. In the measurement process of the horizontal hole fractures in EDZ, since the probe cannot be moved by the self-weight of the probe, a hose was used to tie a soft rope first, and then pass the hose from one end of the hole to the other end, so that the two ends of the rope are placed on both ends of the hole. Then, tie one end of the rope to the probe and pull the probe connected with the data cable

into the borehole from the other end. Finally, the winch slowly collects the cable and measures the image of the hole.

4. Results and Analyses

4.1. Image and Classification. In this study, a total of 14 boreholes were detected for IV grade surrounding rock, including 3 boreholes in the orebody, 4 boreholes in the footwall surrounding rock of the Daxingshan mining area, and 4 boreholes in the orebody, 3 boreholes in the footwall surrounding rock of the Xiaoxingshan mining area. For II

TABLE 2: Summary of the 23 test areas.

Hole number	Location of test area	Location of borehole	Rock type	Rock mass quality
1	20 [#] roadway of -236 m sublevel	Roof	Orebody of Xiaoxingshan	IV
2	Haulage drift at 2 [#] roadway of -236 m sublevel	Roof	Footwall of Daxingshan	IV
3	Haulage drift at 6 [#] roadway of -236 m sublevel	Roof	Orebody of Daxingshan	III
4	Haulage drift at 11 [#] roadway of -236 m sublevel	Roof	Footwall of Daxingshan	IV
5	4 [#] roadway of -236 m sublevel	Roof	Orebody of Daxingshan	II
6	7 [#] roadway of -236 m sublevel	Roof	Orebody of Daxingshan	II
7	9 [#] roadway of -236 m sublevel	Roof	Hanging wall of Daxingshan	III
8	26 [#] roadway of -236 m sublevel	Roof	Orebody of Xiaoxingshan	II
9	26 [#] roadway of -236 m sublevel	Roof	Orebody of Xiaoxingshan	IV
10	29 [#] roadway of -236 m sublevel	Roof	Orebody of Xiaoxingshan	IV
11	Haulage drift of -236 m sublevel	Roof	Footwall of Xiaoxingshan	IV
12	Haulage drift of -236 m sublevel	Roof	Footwall of Xiaoxingshan	III
13	Haulage drift of -236 m sublevel	Roof	Footwall of Xiaoxingshan	IV
14	15 [#] roadway of -218 m sublevel	Roof	Orebody of 3 [#] mining area	III
15	16 [#] roadway of -218 m sublevel	Roof	Orebody of 3 [#] mining area	III
16	17 [#] roadway of -218 m sublevel	Roof	Footwall of 3 [#] mining area	IV
17	11 [#] roadway of -218 m sublevel	Roof	Hanging wall of 3 [#] mining area	IV
18	2 [#] roadway of -218 m sublevel	Sidewall	Orebody of Daxingshan	IV
19	5 [#] roadway of -218 m sublevel	Sidewall	Orebody of Daxingshan	IV
20	15 [#] roadway of -218 m sublevel	Sidewall	Footwall of 3 [#] mining area	IV
21	19 [#] roadway of -218 m sublevel	Sidewall	Orebody of Xiaoxingshan	IV
22	26 [#] roadway of -218 m sublevel	Sidewall	Orebody of Xiaoxingshan	II
23	29 [#] roadway of -218 m sublevel	Sidewall	Orebody of Xiaoxingshan	IV

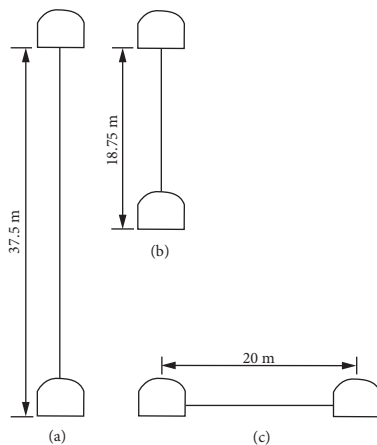


FIGURE 6: Position of EDZ test hole between roadways (a) location of hole No. 1. (b) location of hole No. 2–17. (c) location of hole No. 18–23.

and III grade surrounding rock roadways, a total of 9 boreholes were detected, including 6 boreholes in the orebody of Daxingshan mining area, and 2 boreholes in orebody, 1 borehole in footwall surrounding rock of Xiaoxingshan mining area. Due to the influence of the magnetic field and the presence of silt in the hole, among other reasons, a small part of the images is distorted or unclear and cannot be identified. The obtained images are divided into shotcrete, intact rock mass, joint zone, fracture zone, and broken zone according to the condition of rock and the distribution of fractures within the rock mass. The specific classification criteria and examples are shown in Figure 8.

Hole No. 18 was not counted in the statistics because it was poorly imaged and could not be identified. The borehole wall images of 22 boreholes, No. 1–17 and No. 19–23, and their partition conditions are obtained, which are displayed in the following text according to the classification of IV grade surrounding rock of vertical holes, II and III grade surrounding rock of vertical hole and horizontal hole (Figures 9–11).

Based on the classification images of the above 22 boreholes, the length of each partition and its percentage of the effective length of the corresponding hole were calculated. The results are shown in Table 3.

4.2. Description of Test Results. In the test, due to the initial setting error, test direction, and other reasons, the scale next to the image is not the actual position but only the relative position of that borehole. Therefore, in the latter description, the numbers all represent the position on the scale. The left end of the vertical hole image is on the top, which is called the ‘above,’ and the right end is on the bottom, which is called the ‘below.’ Among the 9 boreholes in the IV grade surrounding rock of the vertical hole, hole No. 1 has a length of 31.7 m from floor of -199 m sublevel to roof of -236 m sublevel. However, due to the image distortion above 19.6 m, the actual effective identifiable length is 12.85 m. According to the borehole images and zoning conditions, the rock mass below 28.2 m is relatively broken and mainly consists of a broken zone and a fracture zone, accompanied by a small part of a joint zone. The intact rock mass zone appears above 28.2 m, and the joint zone and fracture zone alternately appear. The lithology of hole No. 2 is different from other holes; it is granite. The area above 9.8 m is broken, and the broken zone is large. The area below 9.8 m is relatively

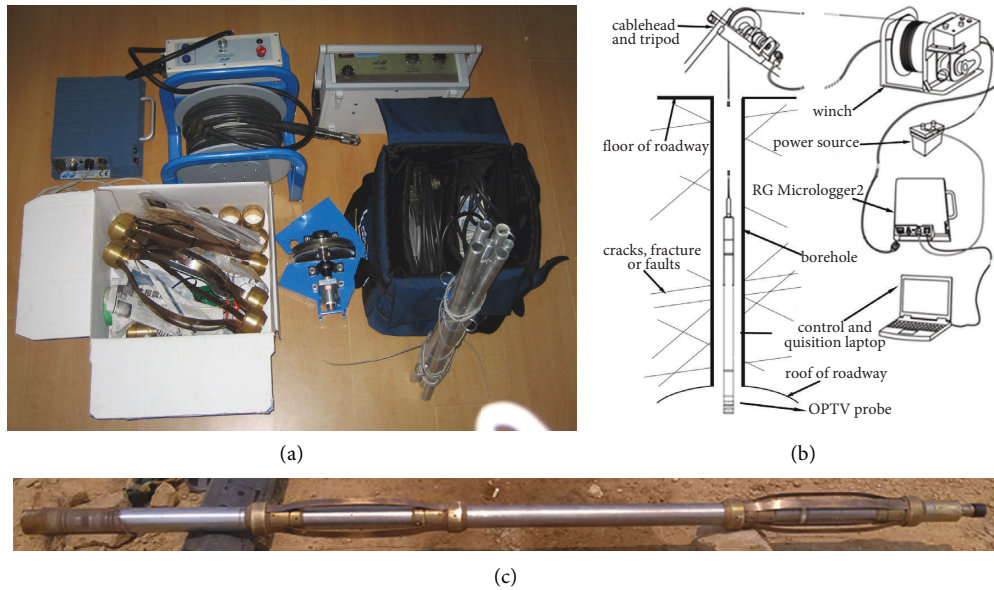


FIGURE 7: Equipment arrangement. (a) Test equipment. (b) Schematic diagram of equipment arrangement. (c) OPTV probe.


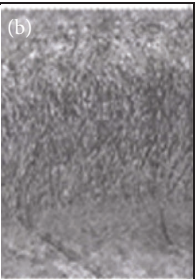
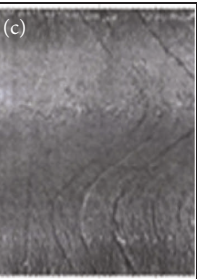
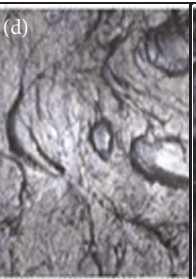

Image example					
Types	Shotcrete	Intact rock mass	Joint zone	Fracture zone	Broken zone
Geological description	Appears at end, obviously different from the other parts	Few joints, the rock mass is not damaged	Lots of parallel joints, fissures intersecting occasionally	Cracks intersect, the rock mass is divided into parts/ Cracks opens to a certain extent	Numerous fissures intersect, the rock mass is partitioned into blocks/ Large cavities appear in the rock mass

FIGURE 8: Classification criteria and examples of surrounding rock (a) shotcrete, (b) intact rock mass, (c) joint zone, (d) fracture zone, and (e) broken zone.

complete, which is mainly the joint zone and fracture zone, and only a small part of the rock mass is broken. Hole No. 4 is relatively broken at both ends of the hole, above 2.4 m and below 9.9 m, and the middle part has more intact rock mass, although there are also broken zones. Hole No. 9 was severely damaged above 4.7 m, and there were many joints and cracks below 10.6 m, but they were basically not damaged. The central part of the rock mass was very intact. Hole No. 10 has a large area of broken zone and fracture zone below 10.2 m, and the rock above 10.2 m is relatively intact with some joints. Hole No. 11 has more broken zone and fracture zone from the overall perspective, but above 2.8 m and below 14.1 m both ends are relatively intact. Hole No. 13 is mainly broken zone and fracture zone above 7.9 m, and there is an

ore-rock interface at 1.85 m. It is relatively complete below 7.9 m, with many joint zones and a few fracture zones. There are some broken zones and fracture zones at hole No. 16 above 3.2 m and below 10.1 m, with more joints and fissures in the middle, and some of the images are distorted and unrecognizable. Hole No. 17 is relatively fractured overall; some are broken, and there is no intact rock mass.

Among the 8 vertical boreholes of II and III grade surrounding rocks, most of hole No. 3 is intact rock mass and joint zone, with more fracture zone below 9.4 m and a broken zone between 15 and -15.3 m. Hole No. 5 is II grade surrounding rock, with intact rock mass and joint zone accounting for the vast majority, a small part of fracture zone and a broken zone of 0.16 m at the lower end. Hole No. 6 is II

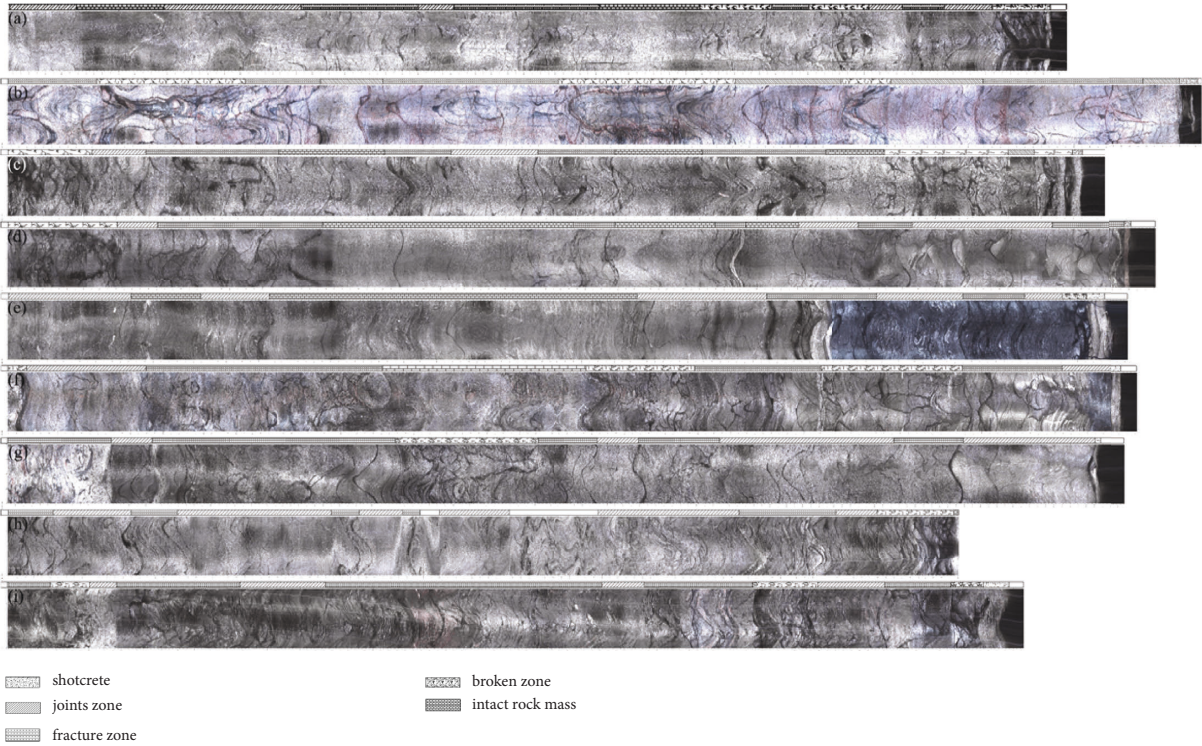


FIGURE 9: Image of IV grade surrounding rock of a vertical hole (a) Hole No. 1. (b) Hole No. 2. (c) Hole No. 4. (d) Hole No. 9. (e) Hole No. 10. (f) Hole No. 11. (g) Hole No. 13. (h) Hole No. 16. (i) Hole No. 17.

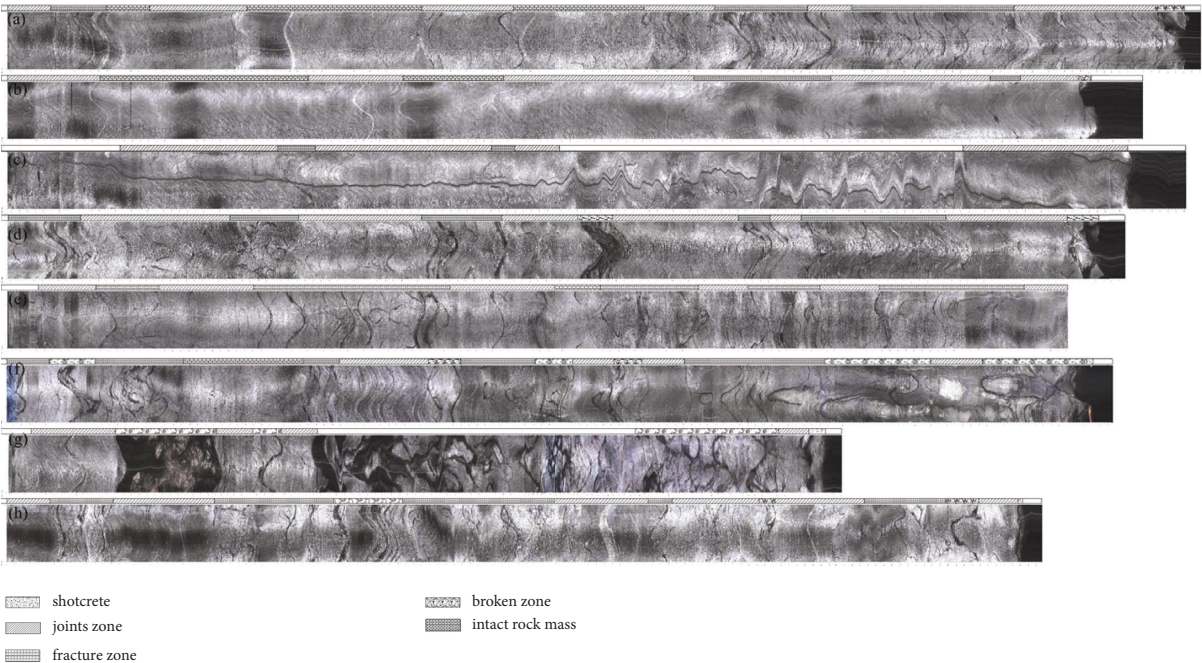


FIGURE 10: Image of II and III grade surrounding rock of vertical hole. (a) Hole No. 3. (b) Hole No. 5. (c) Hole No. 6. (d) Hole No. 7. (e) Hole No. 8. (f) Hole No. 12. (g) Hole No. 14. (h) Hole No. 15.

grade surrounding rock. the image of 7.2–12.2 m is distorted and unrecognizable. The rest of the rock mass is almost joint zone, which is relatively intact. The middle and both ends of hole No. 7 are fractured, and the damage is severe at 8–8.4 m in the middle and 14.1–14.5 m in the lower part. The upper

part of hole No. 8 is relatively intact, the middle part is relatively fractured at 2.2–4.5 m and 6.5–9.2 m, and there are a few cracks in the lower part. Hole No. 12 is very fractured or even broken below 9.2 m, and a intact rock mass, joint zone, and broken zone appear alternately in the middle and

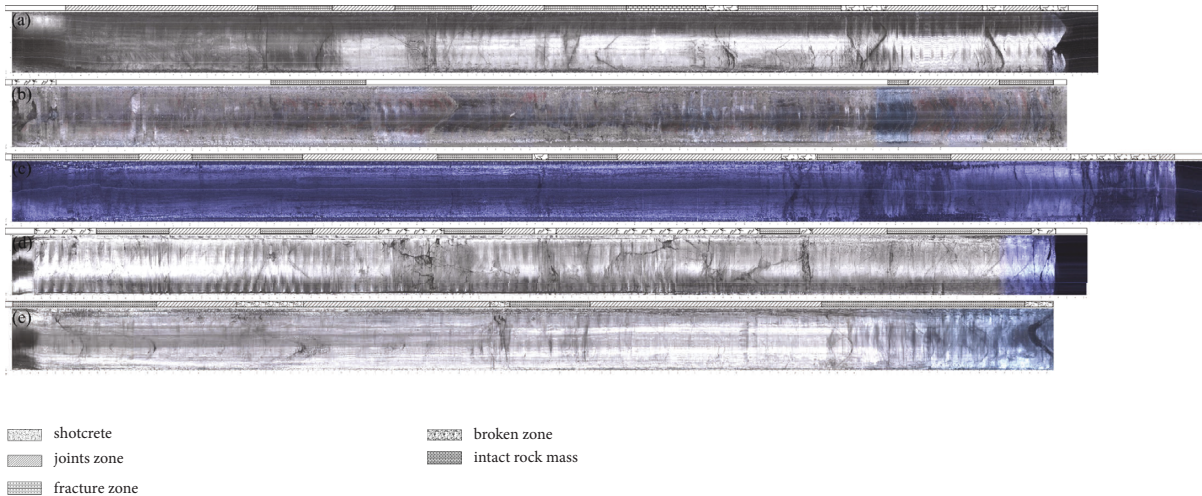


FIGURE 11: Image of horizontal hole. (a) Hole No. 13. (b) Hole No. 20. (c) Hole No. 21. (d) Hole No. 22. (e) Hole No. 23.

TABLE 3: The percentage of effective length of each partition and its percentage in the effective length of corresponding hole.

Hole number	Total length/m	Effective length/m	Intact rock mass/ effective length (%)	Joint zone/ effective length (%)	Fracture zone/ effective length (%)	Broken zone/ effective length (%)
1	31.73	12.85	18.0	31.0	32.8	18.2
2	14.67	14.45	0.0	25.3	43.0	31.7
3	14.74	14.74	29.9	41.4	26.3	2.4
4	13.25	13.12	23.8	15.5	37.7	23.0
5	13.57	13.57	28.6	54.9	15.3	1.2
6	14.04	7.6	0.0	90.0	10.0	0.0
7	13.67	13.67	0.0	57.4	36.6	6.0
8	13.29	12.9	4.7	39.8	55.5	0.0
9	13.86	13.78	36.1	21.5	32.6	9.9
10	13.56	13.3	40.7	41.1	15.9	2.3
11	13.73	13.6	18.5	15.3	41.9	24.3
12	13.61	13.53	11.2	20.8	35.2	32.9
13	13.48	13.4	0.0	35.5	51.3	13.1
14	12.05	6.76	0.0	37.3	0.0	62.7
15	12.75	12.67	0.0	44.8	43.6	11.6
16	11.73	10.34	0.0	63.2	27.9	9.0
17	12.35	12.03	0.0	22.7	63.3	14.0
19	12.56	11.92	7.8	45.7	33.9	12.6
20	12.55	3.62	0.0	29.8	55.8	14.4
21	13.84	13.84	0.0	41.7	46.2	12.1
22	12.41	12.14	0.0	32.0	35.9	32.0
23	12.4	12.4	0.0	47.7	41.9	10.5
Total of IV grade surrounding rock	138.36	116.87	15.7	29.3	38.5	16.5
Total of II and III grade surrounding rock	107.72	95.44	10.9	46.5	30.6	12.0
Total of horizontal hole	63.76	53.92	1.7	41.0	40.8	16.5

upper part. The image above 1.8 m of hole No. 14 is compressed, and 5.6–10.7 m is distorted and cannot be recognized. In other parts, the upper part is mostly a joint zone with a large cavity in the middle, and the lower part is granite, which is seriously broken. In hole No. 15, the fracture zone and joint zone appeared alternately, occasionally partially broken, but the rock mass was intact overall.

Among the five horizontal boreholes, only hole No. 22 is II grade surrounding rock and the other four holes are IV grade surrounding rock. On the whole, hole No. 19 shows the joint zone and fracture zone alternately, and there is a small part of the broken zone at 4.6 m to the right. Because there is silt at the bottom of hole No. 20, most images are not easy to identify, and the rock mass at both ends of the hole is

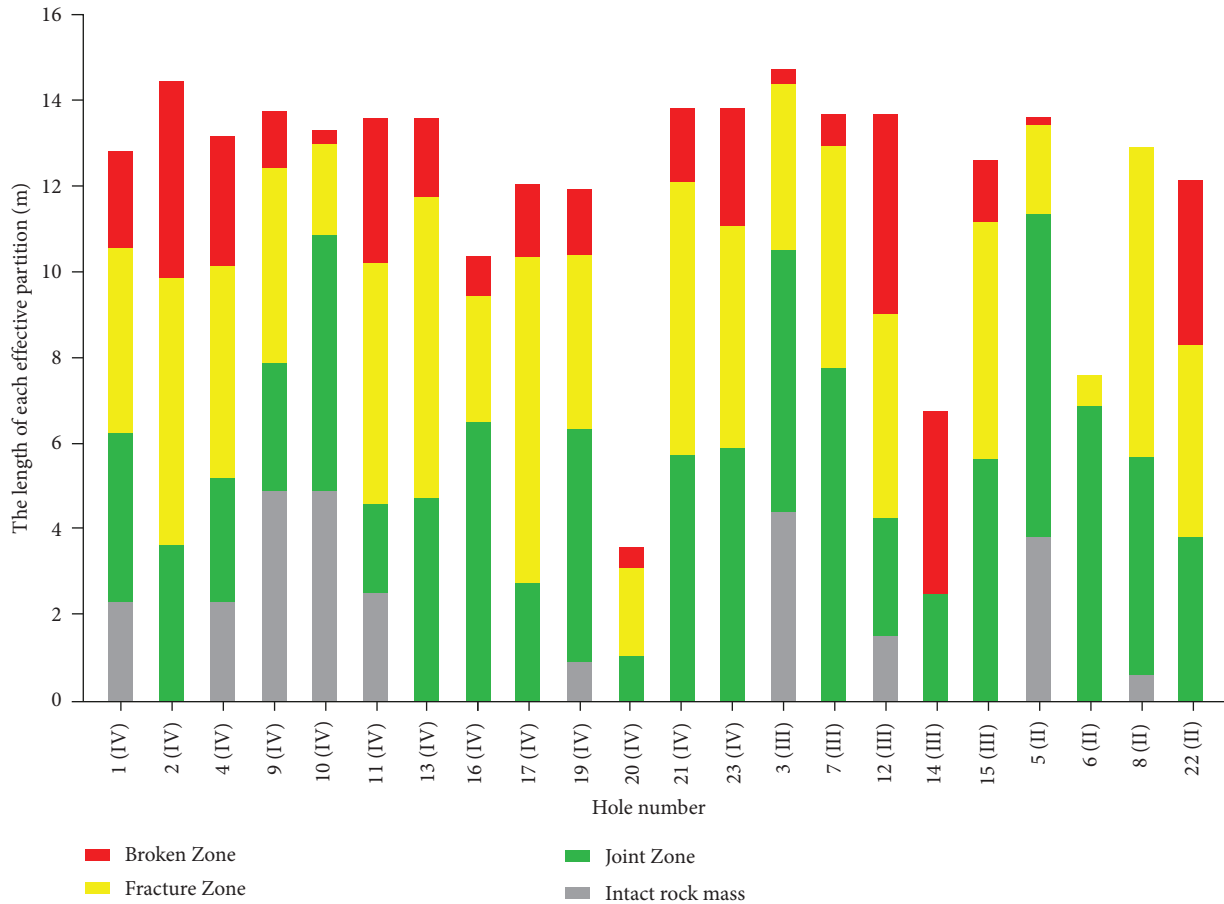


FIGURE 12: The length of each partition of every hole.

relatively fractured and broken. The broken of hole No. 21 is obvious, especially to the right of 5.1 m. There are a large number of broken zone and fracture zone, and large cavities appear in the rock mass. Although hole 22 is II grade surrounding rock, there is a broken zone in the middle and at both ends of the rock mass, but the rock mass is relatively intact except for the broken zone. The right side of 10.5 m and 6.6–7.3 m in the middle of hole No. 23 are relatively fractured, while other parts of the rock mass are relatively intact.

4.3. Cause Analysis. The average identifiable length of IV grade surrounding rock of vertical holes, II and III grade surrounding rock of vertical holes and horizontal holes is 12.99 m, 11.93 m, and 10.78 m respectively, and the percentages of each category are shown in Table 3 and Figure 12. The total percentage of fracture zone and broken zone of II and III grade surrounding rock of vertical holes only represents 42.6% of the total, while these data are 55% and 57%, respectively, in the IV grade surrounding rock of vertical holes and horizontal holes, which is significantly higher than the former. It can be seen that there is a high correlation between the rock mass quality and the broken degree of surrounding rock after excavation. The better the quality of rock mass, the more intact the rock mass is shown in the test

results. Among the five data points of horizontal holes, four are IV grade surrounding rock and one is II grade surrounding rock. Therefore, the influence of rock mass quality is not considered in the comparison with the IV grade surrounding rock of the vertical hole. The percentage of intact rock mass and joint zone in the IV-grade surrounding rock of the vertical hole is similar to that of the horizontal hole, but there is more intact rock mass in the IV-grade surrounding rock of the vertical hole. It is speculated that the horizontal hole is shorter in length (average of 12.8 m compared to an average of 14.5 m for vertical holes) and is more affected by mining vibration.

4.4. Joint Zone in the Roof. Due to equipment limitations, a complete image of the roadway floor was unable to be obtained, but a complete image of the roof could be acquired. According to the literature, the main influence range of mining activities on roadways of similar size is 0.5–2.3 m [11, 12, 34], so further analysis on the roadway roof within 2 m was mainly studied. In the following description, being close to the roadway is called inside, and being away from the roadway is called outside.

Joint zone all appeared within 1.5 m in the 17 vertical holes, of which 15 appeared within 1 m. In the area of 1–2 m close to the roof, a relatively complete joint zone appears,

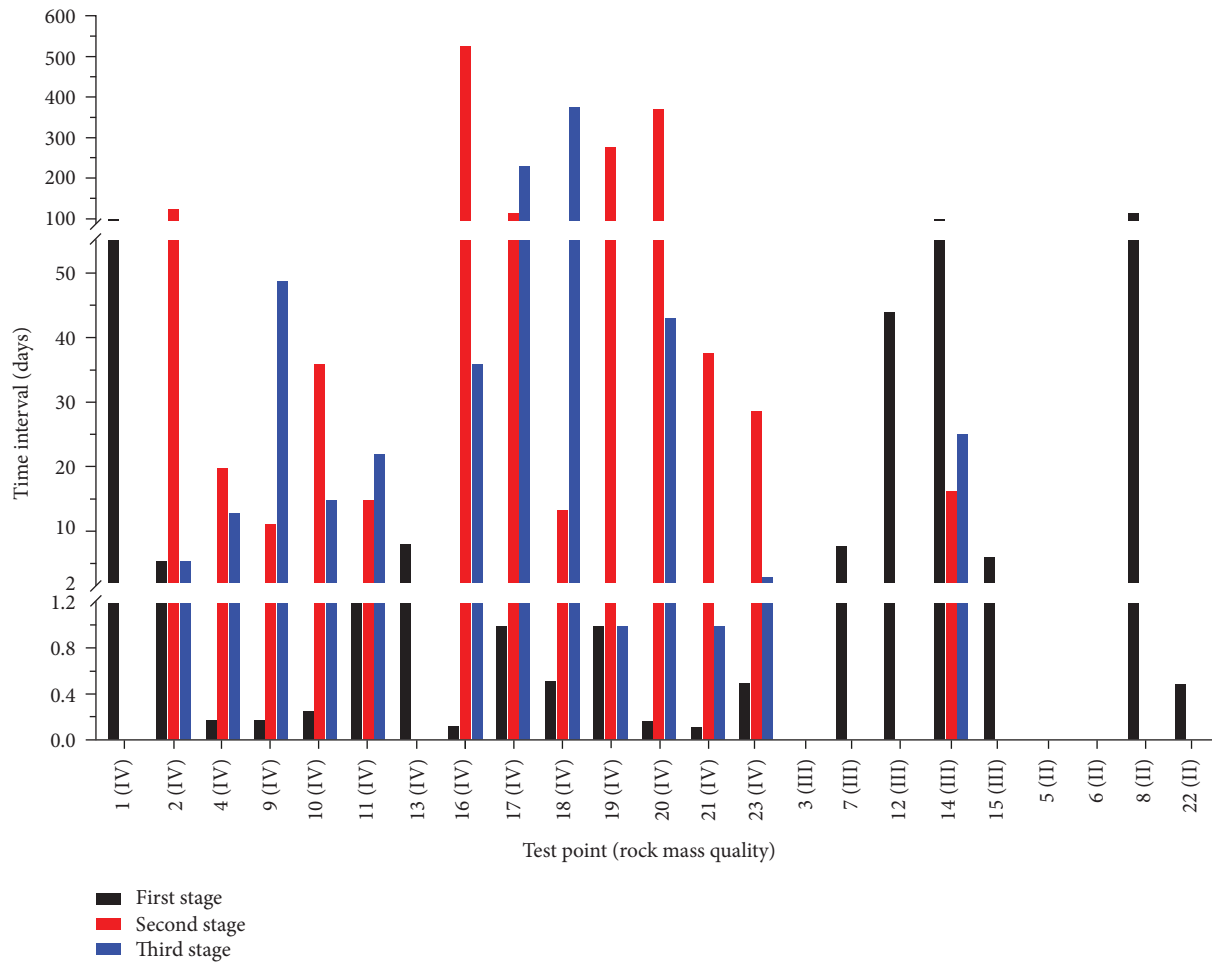


FIGURE 13: Time interval between each supporting measure at each test point (days).

which is caused by the drill and blast method of mining roadway in Xingshan iron mine: At the moment of roadway excavation blasting, the blasting thrust applies pressure to the surrounding area, making the rock mass around the roadway compressed and deformed by the pressure from inside to outside in the radial direction. As the waste rock is thrown out of the roadway, the blasting pressure is suddenly released. While the rock within the roadway boundary becomes an empty area, the original rock stresses on these rock masses are transferred to the rock mass around the roadway, and the rock mass around the roadway is further compressed in the radial direction by the pressure from outside to inside, thus forming the initial joint zone. Some theories believe that there is a self-supporting system during the construction of the roadway, which includes a relaxation zone, transition zone, and compression zone from inside to outside. The compression zone, which is the area where the rock mass is in a state of compressive deformation, is also the basis of the self-supporting system, and this theory is similar to the joint zone theory in this paper [37, 38].

The fracture spacing will be further developed under mining stress and blast vibration if the joint zone receives the expansion space. The developed fractures, together with the expanded weak structural surface of the original rock mass, from a network of fractures cutting the rock mass and

causing the surface rock mass to fracture. On the contrary, if the expansion space is not available, the rock mass will not be cut and fractured. Therefore, the main purpose of support is to protect the joint zone from being destroyed.

5. Optimization of Support System

The main purpose of the cooperation between Xingshan iron mine and us was to propose an effective support system for the roadway to avoid large displacement or rapid failure of the roadway. Therefore, based on the fracture detection results in EDZ in Section 4 of this paper, the support design was made concerning the special geological conditions in each of the mining areas. The Xingshan iron mine recorded the specific time when each support measure was implemented, and the time interval between each support measure at each test point was calculated after the specific time for each support measure at all test points was collected (Figure 13), where the first stage is the time interval between the completion of roadway excavation blasting and the beginning of roadway initial shotcrete; the second stage is the time interval between the completion of roadway initial shotcrete and the beginning of bolt and metal mesh installation; and the third stage is the time interval between the completion of bolt and metal mesh installation and the beginning of

TABLE 4: Support improvement scheme of Xingshan iron mine.

Rock mass quality	IV	III	II
Footwall	<ol style="list-style-type: none"> 1. Shotcrete, bolt, and metal mesh 2. Initial shotcrete within 4 hours after excavation blasting 3. Install bolt and metal mesh within 12 hours after initial shotcrete 4. Secondary shotcrete within 15–20 days after installing bolt and metal mesh 5. Thickness of shotcrete is not less than 140 mm 	<ol style="list-style-type: none"> 1. Shotcrete and bolt 2. Initial shotcrete within 3 days after excavation blasting 3. Install bolt within 14 days after initial shotcrete 4. Thickness of shotcrete is 110–120 mm 	40 mm thick shotcrete
Hanging wall and orebody nearby	<ol style="list-style-type: none"> 1. Shotcrete, bolt and metal mesh 2. Initial shotcrete within 1 day after excavation blasting 3. Install bolt and metal mesh within 7–10 days after initial shotcrete 4. Secondary shotcrete within 20–30 days after installing bolt and metal mesh 5. Thickness of shotcrete is 100–140 mm 	<ol style="list-style-type: none"> 1. Shotcrete and bolt 2. Initial shotcrete within 3–5 days after excavation blasting 3. Install bolt within 7–10 days after initial shotcrete 4. Thickness of shotcrete is 40–100 mm 	—
Most orebody	<ol style="list-style-type: none"> 1. Shotcrete or shotcrete and bolt 2. Initial shotcrete within 7 days after excavation blasting 3. Install bolt within 30 days after initial shotcrete 4. Thickness of shotcrete is 40–80 mm 	—	—

roadway secondary shotcrete. No stage bar indicates that no support measures were carried out later.

Combined with Figure 13 and Table 3, among the 13 test points of IV grade surrounding rock, 9 test points conducted initial shotcrete within 1 day after blasting (first stage within 1 day), and their average percentage of intact rock mass and joint zone accounted for 49%, while the other 4 test points with more than 1 day of first stage accounted for 36%. It can be seen that rapid initial shotcrete has a significant effect on protecting the integrity of surrounding rock. Four test points have carried out bolt and metal mesh within 30 days after initial shotcrete (second stage within 30 days), and their average percentage of intact rock mass and joint zone accounts for 45%. For the other nine test points with the second stage more than 30 days, their average percentage of intact rock mass and joint zone is 45%. Therefore, there is a speculation that the interval between bolt and metal mesh and initial shotcrete becomes less important than the former. It is speculated from Section 4 of this paper that because of the good liquidity of wet shotcrete slurry, mortar and fine materials are highly-rapidly jetted into cracks and joints of rock mass by applying sprayed machine. It develops wedge-effect function through filling the fracture or joint of rock mass, protecting the joint zone from being damaged and greatly improving the integrity of rock mass [39–42]. A similar conclusion can be drawn in III grade surrounding rocks, where the percentage of fracture zone and broken zone is greater when the interval between blasting and initial shotcrete is more than 7 days. While in II grade surrounding rock, such a phenomenon is not very obvious due to the more stable rock mass and fewer samples. Therefore, in IV grade surrounding rocks which is the worst rock mass quality in Xingshan, the broken footwall surrounding rocks should be sprayed by shotcrete within 4 hours after blasting.

The shotcrete will fill the cracks in the rock surface and prevent further development of cracks, protect the joint zone and give it better support ability. The initial shotcrete can be slightly delayed within 4 to 24 hours after blasting for the hanging wall and orebody nearby that has good rock quality, and the initial shotcrete sprayed within 7 days after blasting can ensure the stability of most of the orebody due to the good quality of orebody. The concept of early initial shotcrete is also similar to the concept of the New Austrian tunnelling method (NATM) construction technology.

In the selection of shotcrete thickness, the current shotcrete thickness of Xingshan iron mine is 50–100 mm. The shotcrete effect is good overall, but the shotcrete layer is damaged in some areas. Therefore, in most of the orebody, the selection of 40–100 mm shotcrete thickness is reliable. In the hanging wall and orebody nearby, according to Xingshan iron mine and other engineering experience, increasing the shotcrete thickness to 100–140 mm can effectively ensure that the rock mass and shotcrete are not damaged. In the footwall with the highest degree of fragmentation, the shotcrete thickness must be more than 140 mm to ensure that the joint zone is not damaged. Finally, according to some differences in the grade of surrounding rock in specific parts, the improvement scheme of shotcrete support is proposed.

The footwall of Xingshan iron mine is broken. The orebody of Xingshan iron mine is mostly II and III grade surrounding rocks with better rock mass quality, and when the upper sublevel orebody is mined out, the orebody of this sublevel is decompressed and less pressurized. The hanging wall of Xingshan iron mine is under greater pressure due to the action of the wedge [43]. Therefore, the support method for Xingshan iron mine has been developed, as shown in Table 4. After adopting the new support method, the

roadway has good stability and no significant deformation. At present, it saves a lot of support costs for the Xingshan iron mine.

6. Conclusions

In this study, the fractures in the excavation damaged zone of an underground metal mine were detected, including vertical and horizontal holes. The main conclusions are as follows:

- (1) The images of the detection results were classified as shotcrete, intact rock mass, joint zone, fracture zone, and broken zone. The detection results showed that the total percentages of fracture zone and broken zone of the IV grade surrounding rock are significantly larger than those of II and III grade surrounding rock.
- (2) On the roof of the excavation damaged zone of the roadway, there exists a relatively complete joint zone within 1.5 m of the surrounding rock, which is caused by the roadway excavation using the drill and blast method. The support should ensure that this joint zone is not damaged.
- (3) Based on the actual support method and the result of support, it is concluded that the initial shotcrete support can fill the cracks in the rock surface and prevent further development of cracks, protect the joint zone and make it have better support ability, protect the near-roadway surrounding rock from being damaged. A new support method is thus concluded, and the support has achieved good field results and economic benefits.

Data Availability

The data used to support the findings of this study are available from the corresponding author upon request.

Conflicts of Interest

The authors declare that there are no conflicts of interest.

Acknowledgments

The study was jointly supported by grants from the Key Program of National Natural Science Foundation of China (Grant no. 51534003) and the National Key Research and Development Program of China (Grant no. 2016YFC0801601). The authors are grateful for their support.

References

- [1] G.-L. Feng, X.-T. Feng, and B.-R. Chen, "A microseismic method for dynamic warning of rockburst development processes in tunnels," *Rock Mechanics and Rock Engineering*, vol. 48, no. 5, pp. 2061–2076, 2015.
- [2] G.-L. F. Yang Yu, C.-J. Xu, B.-R. Chen, Da-X. Geng, and Bi-T. Zhu, "Quantitative threshold of energy fractal dimension for immediate rock-burst warning in deep tunnel: a case study," *Lithosphere*, vol. 2022, Article ID 1699273, 2022.
- [3] G.-L. Feng, B.-R. Chen, Y.-X. Xiao et al., "Microseismic characteristics of rockburst development in deep TBM tunnels with alternating soft-hard strata and application to rockburst warning: a case study of the Neelum–Jhelum hydropower project," *Tunnelling and Underground Space Technology*, vol. 122, Article ID 104398, 2022.
- [4] C.-F. Tsang, F. Bernier, and C. Davies, "Geohydromechanical processes in the Excavation Damaged Zone in crystalline rock, rock salt, and indurated and plastic clays—in the context of radioactive waste disposal," *International Journal of Rock Mechanics and Mining Sciences*, vol. 42, no. 1, pp. 109–125, 2005.
- [5] J. Autio, A. Hautojärvi, and J. P. Salo, "The effect of the excavation damaged zone adjacent to the walls of deposition holes on the migration of radionuclides," *MRS Proceedings*, vol. 663, no. 1, p. 645, 2000.
- [6] Z. Hou, "Mechanical and hydraulic behavior of rock salt in the excavation disturbed zone around underground facilities," *International Journal of Rock Mechanics and Mining Sciences*, vol. 40, no. 5, pp. 725–738, 2003.
- [7] A. Mortazavi and H. Molladavoodi, "A numerical investigation of brittle rock damage model in deep underground openings," *Engineering Fracture Mechanics*, vol. 90, pp. 101–120, 2012.
- [8] B. Shen, O. Stephansson, M. Rinne et al., "FRACOD modeling of rock fracturing and permeability change in excavation-damaged zones," *International Journal of Geomechanics*, vol. 11, no. 4, pp. 302–313, 2011.
- [9] B. Pardoën, S. Levasseur, and F. Collin, "Using local second gradient model and shear strain localisation to model the excavation damaged zone in unsaturated claystone," *Rock Mechanics and Rock Engineering*, vol. 48, no. 2, pp. 691–714, 2015.
- [10] S. H. Chen, G. J. Wang, H. Zhou, W. M. Wang, and L. C. Zou, "Evaluation of excavation-induced relaxation and its application to an arch dam foundation," *International Journal for Numerical and Analytical Methods in Geomechanics*, vol. 36, no. 2, pp. 166–181, 2012.
- [11] S. Kwon, C. S. Lee, S. J. Cho, S. Jeon, and W. Cho, "An investigation of the excavation damaged zone at the KAERI underground research tunnel," *Tunnelling and Underground Space Technology*, vol. 24, no. 1, pp. 1–13, 2009.
- [12] L. Malmgren, D. Saiang, J. Toyra, and A. Bodare, "The excavation disturbed zone (EDZ) at Kiirunavaara mine, Sweden - by seismic measurements," *Journal of Applied Geophysics*, vol. 61, no. 1, pp. 1–15, 2007.
- [13] K. Schuster, H. J. Alheid, and D. Boddener, "Seismic investigation of the excavation damaged zone in Opalinus Clay," *Engineering Geology*, vol. 61, no. 2-3, pp. 189–197, 2001.
- [14] S. Kruschwitz and U. Yaramanci, "Detection and characterization of the disturbed rock zone in claystone with the complex resistivity method," *Journal of Applied Geophysics*, vol. 57, no. 1, pp. 63–79, 2004.
- [15] P. Bossart, P. M. Meier, A. Moeri, T. Trick, and J. C. Mayor, "Geological and hydraulic characterisation of the excavation disturbed zone in the opalinus clay of the Mont Terri rock laboratory," *Engineering Geology*, vol. 66, no. 1-2, pp. 19–38, 2002.
- [16] F. Wu, J. Liu, T. Liu, H. Zhuang, and C. Yan, "A method for assessment of excavation damaged zone (EDZ) of a rock mass and its application to a dam foundation case," *Engineering Geology*, vol. 104, no. 3-4, pp. 254–262, 2009.

- [17] P. Blümling, F. Bernier, P. Lebon, and C. Derek Martin, "The excavation damaged zone in clay formations time-dependent behaviour and influence on performance assessment," *Physics and Chemistry of the Earth, Parts A/B/C*, vol. 32, no. 8-14, pp. 588–599, 2007.
- [18] T. Sato, T. Kikuchi, and K. Sugihara, "In-situ experiments on an excavation disturbed zone induced by mechanical excavation in Neogene sedimentary rock at Tono mine, central Japan," *Engineering Geology*, vol. 56, no. 1-2, pp. 97–108, 2000.
- [19] G. Armand, F. Leveau, C. Nussbaum et al., "Geometry and properties of the excavation-induced fractures at the Meuse/Haute-Marne URL drifts," *Rock Mechanics and Rock Engineering*, vol. 47, no. 1, pp. 21–41, 2014.
- [20] M. Cai, P. K. Kaiser, H. Morioka et al., "FLAC/PFC coupled numerical simulation of AE in large-scale underground excavations," *International Journal of Rock Mechanics and Mining Sciences*, vol. 44, no. 4, pp. 550–564, 2007.
- [21] M. Cai and P. Kaiser, "Assessment of excavation damaged zone using a micromechanics model," *Tunnelling and Underground Space Technology*, vol. 20, no. 4, pp. 301–310, 2005.
- [22] S. H. Wang, C. I. Lee, P. G. Ranjith, and C. A. Tang, "Modeling the effects of heterogeneity and anisotropy on the excavation damaged/disturbed zone (EDZ)," *Rock Mechanics and Rock Engineering*, vol. 42, no. 2, pp. 229–258, 2009.
- [23] J. Yang, W. Lu, Y. Hu, M. Chen, and P. Yan, "Numerical simulation of rock mass damage evolution during deep-buried tunnel excavation by drill and blast," *Rock Mechanics and Rock Engineering*, vol. 48, no. 5, pp. 2045–2059, 2015.
- [24] F. Pellet, M. Roosefid, and F. Deleruyelle, "On the 3D numerical modelling of the time-dependent development of the damage zone around underground galleries during and after excavation," *Tunnelling and Underground Space Technology*, vol. 24, no. 6, pp. 665–674, 2009.
- [25] S. Kamewada, H. Gi, and S. Taniguchi, "Application of borehole image processing system to survey of tunnel," *International Symposium on Rock Joints*, pp. 51–58, 1990.
- [26] X.-J. Hao, X.-T. Feng, C.-X. Yang, Q. Jiang, and S. J. Li, "Analysis of EDZ development of columnar jointed rock mass in the Baihetan diversion tunnel," *Rock Mechanics and Rock Engineering*, vol. 49, no. 4, pp. 1289–1312, 2016.
- [27] S. J. Li, X.-T. Feng, C. Y. Wang, and J. A. Hudson, "ISRM suggested method for rock fractures observations using a borehole digital optical televiewer," *Rock Mechanics and Rock Engineering*, vol. 46, no. 3, pp. 635–644, 2013.
- [28] X.-T. Feng, X.-J. Hao, Q. Jiang, S. J. Li, and J. A. Hudson, "Rock cracking indices for improved tunnel support design: a case study for columnar jointed rock masses," *Rock Mechanics and Rock Engineering*, vol. 49, no. 6, pp. 2115–2130, 2016.
- [29] S. Li, X. Feng, Z. Li et al., "In situ experiments on width and evolution characteristics of excavation damaged zone in deeply buried tunnels," *Science China Technological Sciences*, vol. 54, no. S1, pp. 167–174, 2011.
- [30] S. Li, X.-T. Feng, Z. Li, C. Zhang, and B. Chen, "Evolution of fractures in the excavation damaged zone of a deeply buried tunnel during TBM construction," *International Journal of Rock Mechanics and Mining Sciences*, vol. 55, pp. 125–138, 2012.
- [31] X.-T. Feng, H.-S. Guo, C.-X. Yang, and S. J. Li, "In situ observation and evaluation of zonal disintegration affected by existing fractures in deep hard rock tunneling," *Engineering Geology*, vol. 242, pp. 1–11, 2018.
- [32] H.-S. Guo, X.-T. Feng, S.-J. Li, C. X. Yang, and Z. B. Yao, "Evaluation of the integrity of deep rock masses using results of digital borehole televiewers," *Rock Mechanics and Rock Engineering*, vol. 50, no. 6, pp. 1371–1382, 2017.
- [33] B. Tang, H. Cheng, Y. Tang et al., "Excavation damaged zone depths prediction for TBM-excavated roadways in deep collieries," *Environmental Earth Sciences*, vol. 77, no. 5, p. 165, 2018.
- [34] H. Wang, Y. Jiang, S. Xue et al., "Assessment of excavation damaged zone around roadways under dynamic pressure induced by an active mining process," *International Journal of Rock Mechanics and Mining Sciences*, vol. 77, pp. 265–277, 2015.
- [35] H.-B. Li, M.-C. Liu, W.-B. Xing, S. Shao, and Jw Zhou, "Failure mechanisms and evolution assessment of the excavation damaged zones in a large-scale and deeply buried underground powerhouse," *Rock Mechanics and Rock Engineering*, vol. 50, no. 7, pp. 1883–1900, 2017.
- [36] N. Xu, F. Dai, B. Li, Y. Zhu, T. Zhao, and D. Yang, "Comprehensive evaluation of excavation-damaged zones in the deep underground caverns of the Houziyan hydropower station, Southwest China," *Bulletin of Engineering Geology and the Environment*, vol. 76, no. 1, pp. 275–293, 2017.
- [37] S. Zhong, "On Tunnel Design and Construction Guaranteed by Correct Concept and New Techniques," *2014 China Tunnel And Underground Construction*, pp. 77–85, 2014.
- [38] S. Zhong, "The formation and developing of self-supporting system in the surrounding rock of a tunnel," *Journal of Railway Engineering Society*, vol. 9, pp. 678–684, 1994.
- [39] I. Galan, A. Baldermann, W. Kusterle, M. Dietzel, and F. Mittermayr, "Durability of shotcrete for underground support—Review and update," *Construction and Building Materials*, vol. 202, pp. 465–493, 2019.
- [40] T. Stacey, "Shotcrete in mines—state-of-the-art in South Africa," *Proc. Int. Seminar and Field Trials on Mine Surface Support Liners Section*, pp. 22–24, 2001.
- [41] G. Methven, *In-cycle Application of Fibre Reinforced Shotcrete*, "Shotcrete: More Engineering Developments," CRC Press, Boca Raton, Florida, United States, 2004.
- [42] L. Li, A.-X. Wu, Y.-M. Wang, B. Han, H. Wang, and C. Wang, "Mechanism of wet shotcrete interacting with rock in support systems," *Journal of Central South University*, vol. 20, no. 3, pp. 821–829, 2013.
- [43] R. He, J. Zhang, Y. Liu, D. Song, and F. Ren, "Determination of the ultimate underground mining depth considering the effect of granular rock and the range of surface caving," *Mathematical Problems in Engineering*, vol. 2021, Article ID 5576786, pp. 1–16, 2021.